AIMS Materials Science, 11(5): 1013–1034.
DOI: 10.3934/matersci.2024048
Received: 22 August 2024
Revised: 08 October 2024
Accepted: 11 October 2024
Published: 28 October 2024

http://www.aimspress.com/journal/Materials

Research article

Research of joining the SiC and Cu combination by use of SnTi solder filled with SiC nanoparticles and with active ultrasound assistance

Tomas Melus[1,*], Roman Kolenak[1], Jaromir Drapala[2], Mikulas Sloboda[1], Peter Gogola[1] and Matej Pasak[1]

[1] Faculty of Materials Science and Technology in Trnava, Slovak University of Technology in Bratislava, Jána Bottu No. 2781/25, 917 24 Trnava, Slovak Republic
[2] Faculty of Materials Science and Technology, Technical University of Ostrava, 17. Listopadu 15, 708 33 Ostrava, Czech Republic

* **Correspondence:** Email: tomas.melus@stuba.sk.

Abstract: The aim of this study was to characterize a Sn-Ti solder alloy containing 6 wt.% SiC nanoparticles and evaluate its use for direct soldering of SiC ceramics to a copper (Cu) substrate. Soldering was performed with direct ultrasound activation. The average tensile strength of the solder alloy was 17.1 MPa. Differential Thermal Analysis (DTA) analysis revealed an apparent transition at 234 °C, corresponding to a eutectic reaction within the Sn-Ti binary system, indicating structural changes in the solder. The solder matrix consisted primarily of pure tin, while titanium combined with SiC nanoparticles to form a TiC phase. The existence of this phase was confirmed by energy dispersive X-ray spectroscopy (EDX) and X-ray diffraction (XRD) analysis of the solder. The bond at the interface between the SiC ceramic substrate and the solder was formed through diffusion and chemical reactions. The XRD analysis of the fractured surface from the SiC side confirmed the formation of phases such as TiC, Ti_2Sn, CTi_2, CuSn, SiC, and Cu_6Sn_5; the TiC and CTi_2 phases resulted from the interaction of active Ti in the solder with the SiC ceramic surface. The bond at the Cu substrate interface formed due to the high solubility of tin in the solder and the formation of probable CuSnTi and $CuSnTi3_5$ phases, along with a mixture of Sn + η Cu_6Sn_5 solid solution. The average shear strength of the SiC/Cu joint, fabricated using SnTi3 solder with 6 wt.% SiC nanoparticles, was 21.5 MPa.

Keywords: SiC ceramic; soldering; Cu substrate; nanoparticles SiC; Sn-Ti solder; ultrasonic soldering

1. Introduction

Soldering alloys are very important in the electronic industry since they are used for soldering electronic components such as printed circuit boards [1–4]. Tin-based, lead-free solders have been used in the electronic industry for several years in order to eliminate the negative effects of lead on human health and the environment [5–9] However, the higher melting point of these solders requires higher soldering temperatures, which often leads to a percentual increase in soldering defects. These defects are often caused by deteriorated wettability, which unfavorably affects the electric and mechanical properties of joints. In order to mitigate those issues, the majority of soldering alloys contain a low percentage of other elements such as silver (Ag), antimony (Sb), and copper (Cu), which improve the overall properties of solder [10–14].

The solder alloys Sn-52In and Sn-58Bi show low melting points and have, for a long time, been used for gradual soldering and for heat-sensitive devices. However, the high price of indium and the fragility of Sn-58Bi solder limit their further expansion. Therefore, the development of new soldering materials that offer good mechanical and electrical properties and low melting points is necessary.

Researchers have been trying to solve this issue by introducing special nanoparticles into traditional solders, thus developing new types of composite solders. This innovative approach significantly enhances the solder properties and mitigates the imperfections currently occurring at higher soldering temperatures [15].

Ultrasonic activation is often used in soldering because it can greatly improve the mechanical properties and microstructure of joints. This process uses a piezoelectric oscillator that creates vibrations, resulting in a more even distribution of solder and better penetration into the materials. A study [16] demonstrated that ultrasonic processing can have a positive effect on the mechanical properties and microstructure evolution of Cu/SAC305 solder joints.

In [17], researchers added SiC nanoparticles to a Sn58Bi solder to develop a new composite solder, showing a 6% increase in shear strength. The thickness of the intermetallic compound was almost identical for both the Sn58Bi and Sn58Bi + SiC specimens. The Sn58Bi + SiC solder exhibited finer eutectic structures and smaller grain size than the Sn58Bi solder without SiC nanoparticles.

The authors of [18] systematically studied the effects of adding titanium (Ti) nanoparticles to a Sn58Bi solder on the melting process, wettability, shear strength, and growth of intermetallic compounds (IMC). The results showed that the addition of Ti nanoparticles significantly improved the wettability and shear strength of the Sn58Bi solder, while the optimum content of Ti addition was 0.1 wt.%. The microstructure of the Sn58Bi solder was distinctly refined by the presence of Ti nanoparticles, which also significantly reduced the thickness of the interphase IMC. However, this addition just slightly affected its melting point. In addition, the IMC thickness in the Sn58Bi/Cu boundary was distinctly higher than that of the Sn58Bi-0.Ti/Cu solder after multiple remelting, which suggests that the addition of Ti nanoparticles could suppress the growth of IMC in the solder/Cu boundary after several remelting.

Researchers have also looked at the effect of special nanoparticles on the properties of solders. For example, a study [19] demonstrated that Ni-modified multi-wall carbon nanotubes (MWCNTs) have a significant effect on the shear strength and microstructure of Sn-3.0Ag-0.5Cu solder joints. The addition of these nanoparticles resulted in finer grain size, more uniform phase distribution, and slower growth of IMCs at the solder–substrate interface. These results support that the introduction of special

nanoparticles into traditional solders not only improves their mechanical properties but also contributes to their long-term reliability.

In [20], it was revealed that the shear strength of a Sn-Ag joint can be increased by the addition of nanostructural particles of polyhedral oligomeric silsesquioxanes (POSS). The technology of nanostructural POSS materials with suitable organic groups can support the bonding between nano-reinforcements and the metallic matrix. The study proved that the addition of nanoparticles to a conventional soldering alloy, with the aim of developing a kind of composite solder, successfully improves the mechanical properties of soldered joints.

The authors of [21] studied the reactive wetting properties of the Sn2Ti alloy on polycrystalline diamond (PCD) substrates, which are made of multi-crystalline diamond grains produced at different temperatures. The cobalt content in the substrates influenced the initial wetting temperature: an increase in Co content lowered that parameter. The isothermal results showed that the substrates with 12% Co were well-wetted at 700 °C due to the formation of IMC compounds of CoSnTi and the adsorption of Ti. When the wetting temperature exceeded approximately 800 °C, the adsorption of titanium at the boundary and the formation of interphase compounds and titanium carbide were responsible for the reactive wetting of the Sn-2Ti alloy on PCD substrates.

This work evaluated the mixture of the solder alloy SnTi3 with 6 wt.% of SiC nanoparticles, analyzing the ultrasonic soldering of SiC ceramics and a Cu substrate. The SnTi3 alloy was selected due to its potential to improve both the mechanical and thermal properties of solder joints, while the addition of SiC nanoparticles aims to increase the microstructure and bond strength. Ultrasonic activation further promotes better wettability and uniform distribution of the solder. In this study, we investigate the microstructure, phase composition, phase transition temperatures, and tensile strength of the solder joints. The interaction between the solder and the substrate surface was analyzed to evaluate the bonding mechanisms. In addition, shear strength tests were performed to evaluate the mechanical properties of the solder joints. This research contributes to the advancement of composite solder joints for high-demand applications, while providing insight into the microstructural benefits of the addition of SiC nanoparticles.

2. Materials and methods

The pre-alloy SnTi3 was prepared in a ceramic crucible in a vacuum induction oven. Prior to melting, the chamber was evacuated, and the material was melted. After full melting, argon was supplied to the chamber, and the alloy was then cast into a prepared steel mold. Alloy production was subsequently performed in a vacuum induction oven. The prepared pre-alloy SnTi3 was melted in a crucible without a vacuum, and argon gas was supplied into the crucible. After full melting, the nanoparticles were forced into a capsule of the desired weight. The melt was subsequently mechanically stirred with a quartz stick and cast into a steel mold.

Chemical analysis was performed by atomic emission spectrometry with induction coupled plasma (ICP-AES), also known as optical emission spectrometry with induction coupled plasma (ICP-OES). The measured results are shown in Table 1. This analytic technique is used for the detection of chemical elements and was conducted on a SPECTRO VISION EOP instrument. It is a type of emission spectrometry that uses inductively coupled plasma to generate excited atoms and ions, which emit electromagnetic radiation at wavelengths characteristic of specific elements.

Table 1. Composition of SnTi3 solder + 6 wt.% SiC nanoparticles using the ICP-AES method and the planar analysis type energy dispersive X-ray spectroscopy (EDX) (wt.%).

Alloys	Analysis type	Sn	Ti	Si	C	nano SiC
SnTi3 + 6 wt.% SiC nanoparticles	Weighing	-	3	-	-	6
	ICP-AES	-	2.37	-	-	6.1

The melting point of the solder alloy was measured by differential thermal analysis (DTA). This analysis was performed on a DTA SETARAM Setsys 18TM. DTA analyses were performed under the following conditions: air atmosphere (purity 5N), air flow rate: 50 mL/min, temperature increment: 5 °C/min. These temperatures were recorded and analyzed using the SETSOFT software. The temperatures of phase transformations within the liquid–solid range were evaluated by DTA curves.

The X-ray diffraction (XRD) analysis was performed on metallic sawdust from the cast and annealed specimens of solder alloys using the X-ray diffractometer PANalytical Empyrean Malvern Panalytical Ltd., Malvern, UK. This measuring procedure, employing metallic sawdust, was selected in order to eliminate the effect of casting texture on the recorded XRD image. The measurements were conducted in Bragg-Brentano geometry.

The theta–two theta angle ranged from 20 to 145°. The source of XRD was a co-anodic lamp set to 40 kV and 40 mA power. The impinging beam was modified by the Soller's slit 0.04 rad, 1/4° divergence slit, and 1/2° anti-scatter slit. The path of the diffracted beam was provided with a 1/2° anti-scatter slit, 0.04 rad Soller's slit, Fe beta filter, and a PIXcel3D position-sensitive detector operating in 1D scanning regime. The quality of the phase was analyzed by the PANalytical Xpert High Score (HighScore Plus version 3.0.5) software with the ICSD FIZ Karlsruhe database.

The mechanical test measured the tensile strength of the active solder alloy SnTi3 with 6 wt.% SiC nanoparticles. Three test pieces were used to measure the tensile strength of the experimental solder, standardized in shape and dimensions. The test pieces were flat and 4 mm in thickness. The tensile strength was measured on the versatile tearing machine LabTest 5.250SP1-VM. The loading rate of the specimens was set to 1 mm/min.

The microstructure was assessed by the electron scanning microscope JEOL JSM 7600F (scanning electron microscopy/energy dispersive X-ray spectroscopy, Jeol Ltd., Tokio, Japan), employing the electron source with Schott's emission field, operating at 20 kV and 90 μA. The specimens were placed at a working distance of 15 mm and documented by the detector of reverse scatter of electrons. The analysis of chemical elements was performed by a silicon drift detector, Oxford Instruments X-Max, an energy dispersion X-ray spectrometer (type EDS, Oxford Instruments plc, Abington, UK).

Soldering was performed with substrates of the following dimensions:

- SiC ceramics in the form of a disk with diameter ø 15 × 3 mm;
- Cu material in the form of a disk with diameter ø 15 × 3 mm;
- Cu material in the form of a square with dimensions 10 × 10 × 3 mm.

Figure 1a shows the scheme of a soldered joint for analysis of solder/substrate boundaries; the scheme for measurement of shear strength is shown in Figure 1b.

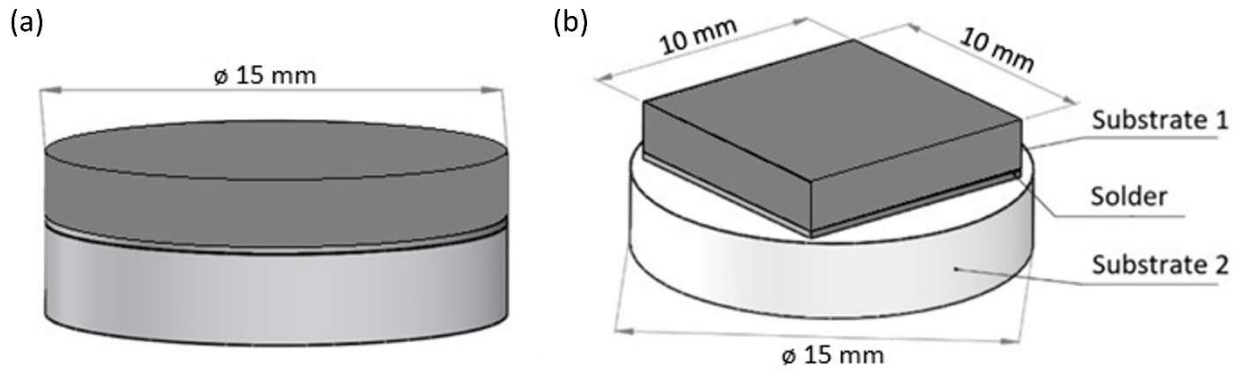

Figure 1. Soldered joint assembly (a) for analysis of solder/substrate boundary, and (b) for shear strength measurement.

Solder activation was performed by the ultrasonic equipment Hanuz UT2-ultrasonic transducer, employing an oscillation piezo-electric system with a titanium sonotrode, 3 mm in diameter. The ultrasound parameters are given in Table 2. Heating of the solder was performed using the hot plate CERAN 500.

Table 2. Ultrasound parameters.

Ultrasonic power	Operating frequency	Amplitude	Soldering temperature	Ultrasonic duration
400 W	40 kHz	2 μm	300 °C	5 s

The substrates were first gently machined to remove surface oxides, ensuring a clean surface for optimum adhesion. Subsequently, a thorough degreasing of the Al_2O_3 and Cu substrates was performed using denatured alcohol to remove any impurities. After degreasing, the substrates were placed on a hot plate. The hot plate temperature was set at 300 °C. Heating was carried out for 200–300 s to ensure uniform temperature and good melting of the SnTi3 solder with 6 wt.% SiC nanoparticles. Once the desired temperature was reached, a small amount of solder was deposited on the surface of the substrate.

Then, the sonotrode of the ultrasonic device was immersed in the molten solder for 5 s. Due to the ultrasonic waves, the solder was activated, leading to the disruption of the oxides in the solder alloy, which subsequently reached the surface of the solder. Subsequently, the prepared substrates were bonded to the molten solder to form a joint. The joints were then cooled at room temperature for 10–20 s. Figure 2 shows a schematic of the ultrasonic brazing process. The metallographic preparation consisted of grinding and polishing processes and etching of embedded specimens. The specimens were mounted in a jig on a grinding machine. Grinding was performed using diamond emery papers with grain sizes of 600, 1200, and 2400 g.

During the grinding process, water was supplied on emery papers, ensuring the washing out of formed debris. The grinding process with each emery paper lasted for 3 min. After grinding of specimens, polishing was performed using polishing disks with diamond emulsions with particle sizes of 9, 6, 3, and 1 μm. Polishing lasted 10 min for each emulsion. After grinding and polishing the specimens, carbon coating was performed to ensure a conductive surface for the SEM equipment.

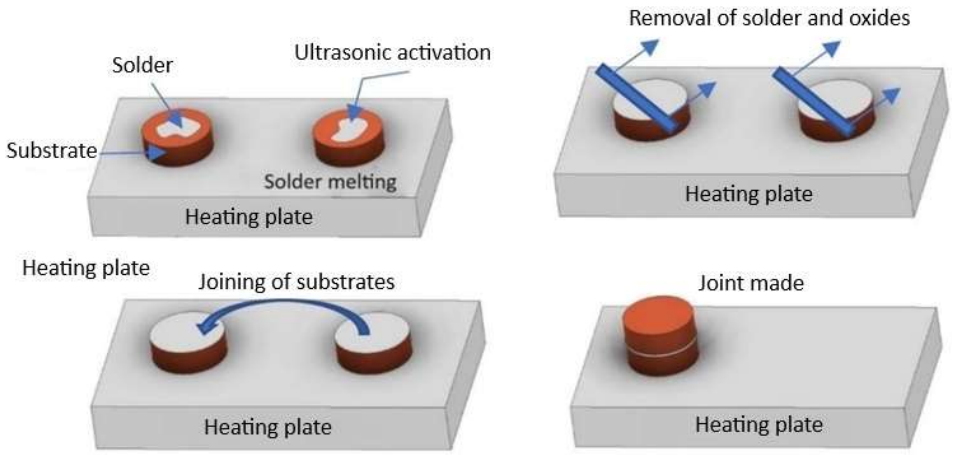

Figure 2. Schematic representation of ultrasonic soldering.

The shear strength was measured on the versatile tearing machine LabTest 5.250SP1-VM. The jig with a defined shape of the test specimen (Figure 3) was used for directional change of loading force acting on the test specimen. This shearing jig ensures a uniform shear load in the solder/boundary plane. Three joints were used for shear strength measurement.

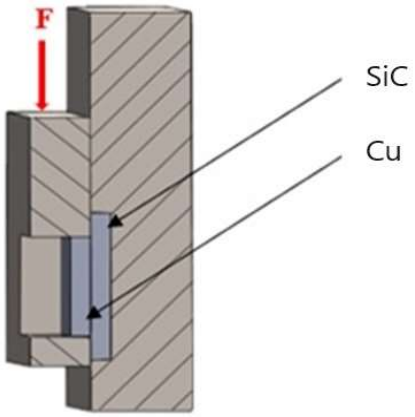

Figure 3. Schematic representation of a jig for shear strength measurement.

3. Results and discussion

3.1. DTA analysis

The DTA analysis of the SnTi3 solder with 6 wt.% SiC nanoparticles is shown in Figure 4 (heating). This shows the existence of two significant thermal transformations in soldering alloys. The first transformation takes place at the temperature of 234 °C, where initial changes in solder microstructure occur. This can be associated with the eutectic reaction, which corresponds to the eutectic reaction in the Sn-Ti binary system.

The other transformation indicates the end of melting, which occurs at 244 °C. This may be the result of the total dissolving of intermetallic alloys or the next phase transformation, which affects the

mechanical and physical properties of solder. The solder matrix consists of tin, where irregular grey constituents are visible, forming the intermetallic TiC phase.

The findings from the DTA analysis and microstructural images provide a comprehensive view of the thermal and structural stability of SnTi3 + 6 wt.% SiC nanoparticles, which may be essential for its usage in different industrial applications.

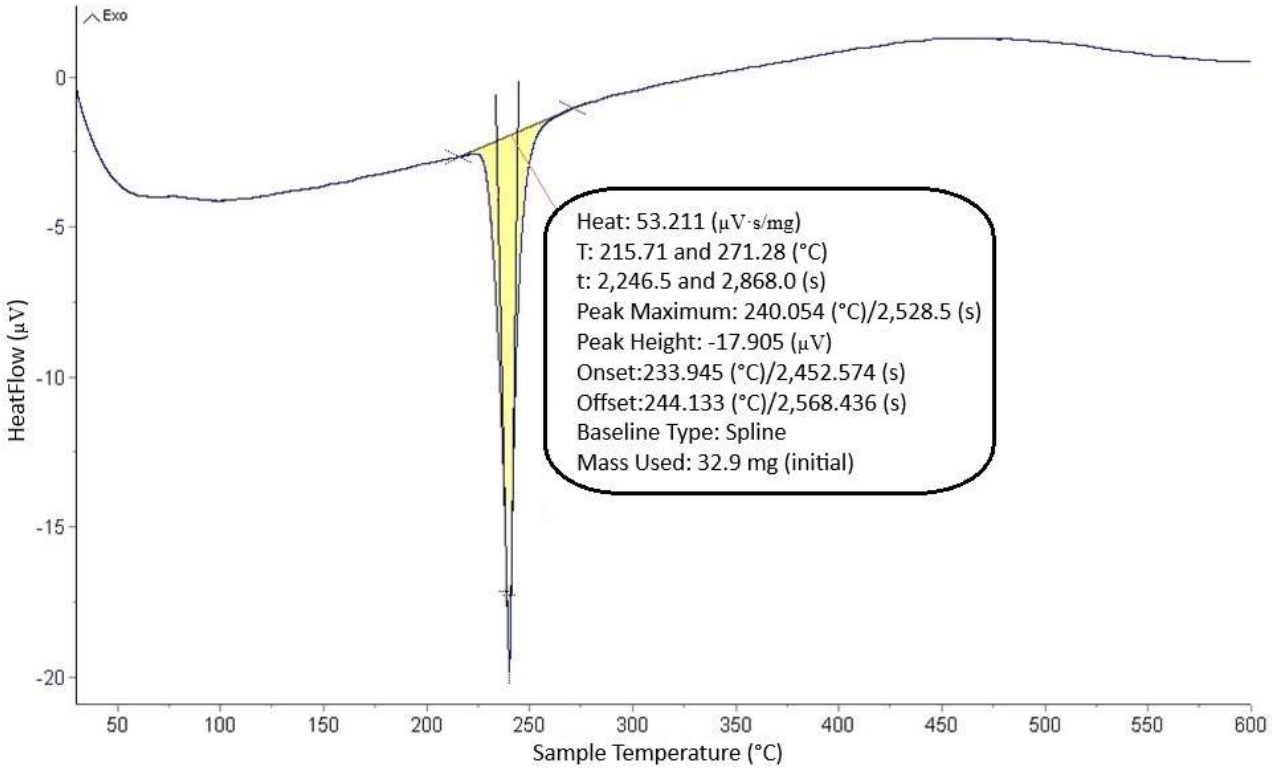

Figure 4. DTA analysis of the SnTi3 solder with 6 wt.% SiC nanoparticles at a heating rate of 5 °C/min.

3.2. Microstructure analysis

In order to determine the chemical composition and identify individual phases, the SEM/EDX analysis was performed on the experimental SnTi3 + 6 wt.% SiC nanoparticles (Figure 5). Spectra 1–5, shown in Table 3, were analyzed. The great dark irregular constituents occurring in Spectrum 1 contained approximately 75 wt.% Si and 25 wt.% C, which corresponds stoichiometrically to the Si_3C phase. Spectrum 2 represents tiny dark polygonal constituents, corresponding to the intermetallic SiC phase in a 1:1 ratio of Si to C. The analysis of Spectrum 3 showed that a metastable Si_2C_3 phase may be related. Spectrum 4 can be unanimously defined as a stoichiometric intermetallic phase of TiC with a 1:1 proportion of Ti:C. This phase is stable at titanium concentrations between 50 and 60 wt.% Ti; therefore, there was a direct interaction of titanium with carbon from the ceramic material. Spectrum 5 represents the zone of the solder matrix with pure tin. The particles containing Si and C situate irregularly in the structure, often creating big clusters of irregular shape with slightly rounded edges. Two kinds of Si_3C carbides were observed, together with possibly Si_2C_3.

Microstructural analysis showed that the distribution of phases, such as TiC and clusters of SiC nanoparticles, had a significant impact on the mechanical properties of the joint. Smaller and uniformly distributed structures improve the tensile and shear strength of the material. Conversely, clusters of irregular shape and size can locally weaken the mechanical properties of the joint. This correlation between microstructure and mechanical properties indicates that a finer microstructure, composed of uniformly distributed SiC particles and TiC phases, contributes to higher strength and toughness of the joint, thereby increasing its resistance to failures.

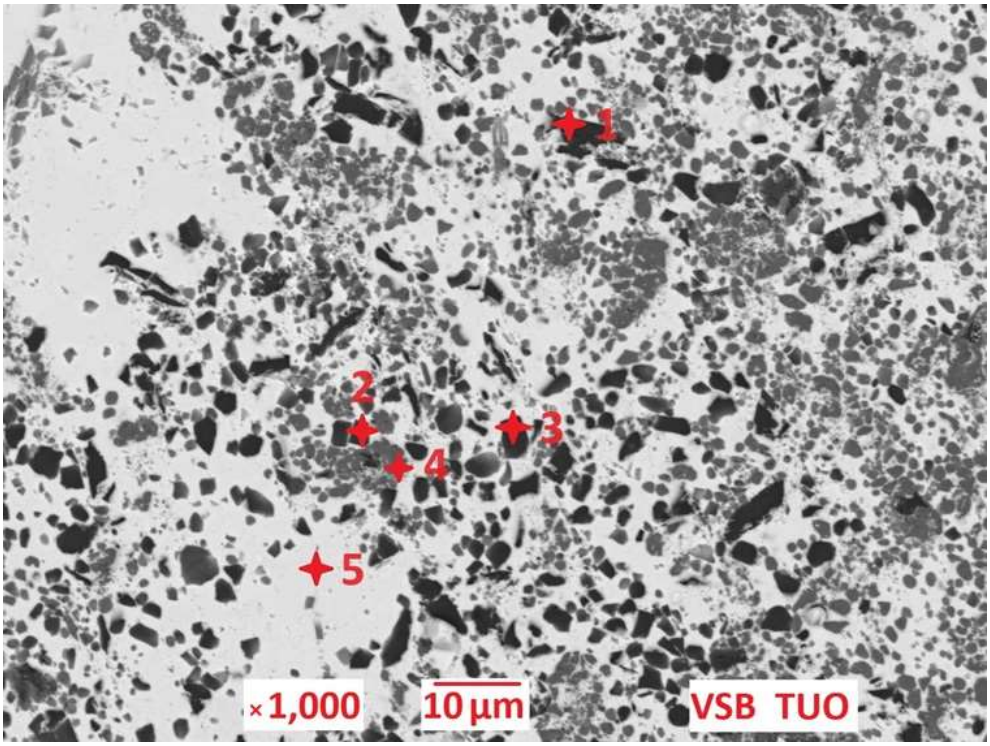

Figure 5. Microstructure of SnTi3 + 6 wt.% SiC nanoparticles.

Table 3. Results from SEM/EDX point analysis performed on SnTi3 solder with 6 wt.% SiC nanoparticles.

Spectrum	C (wt.%)	Si (wt.%)	Ti (wt.%)	Sn (wt.%)	Solder component
1	23.9	75.2	-	0.9	Phase Si_3C
2	45.2	45.2	0.7	9.0	Intermetallic phase SiC
3	61.5	37.6	-	1.0	Metastatic phase Si_2C_3
4	46.8	1.5	50.3	1.4	Intermetallic phase TiC
5	-	-	-	100.0	Matrix Sn

The XRD measurement was performed using a dispersion X-ray spectrometer on the specimens prepared from solder volume. The XRD analysis of solder proved the presence of intermetallic phase type TiC. The record from diffraction analysis is documented in Figure 6.

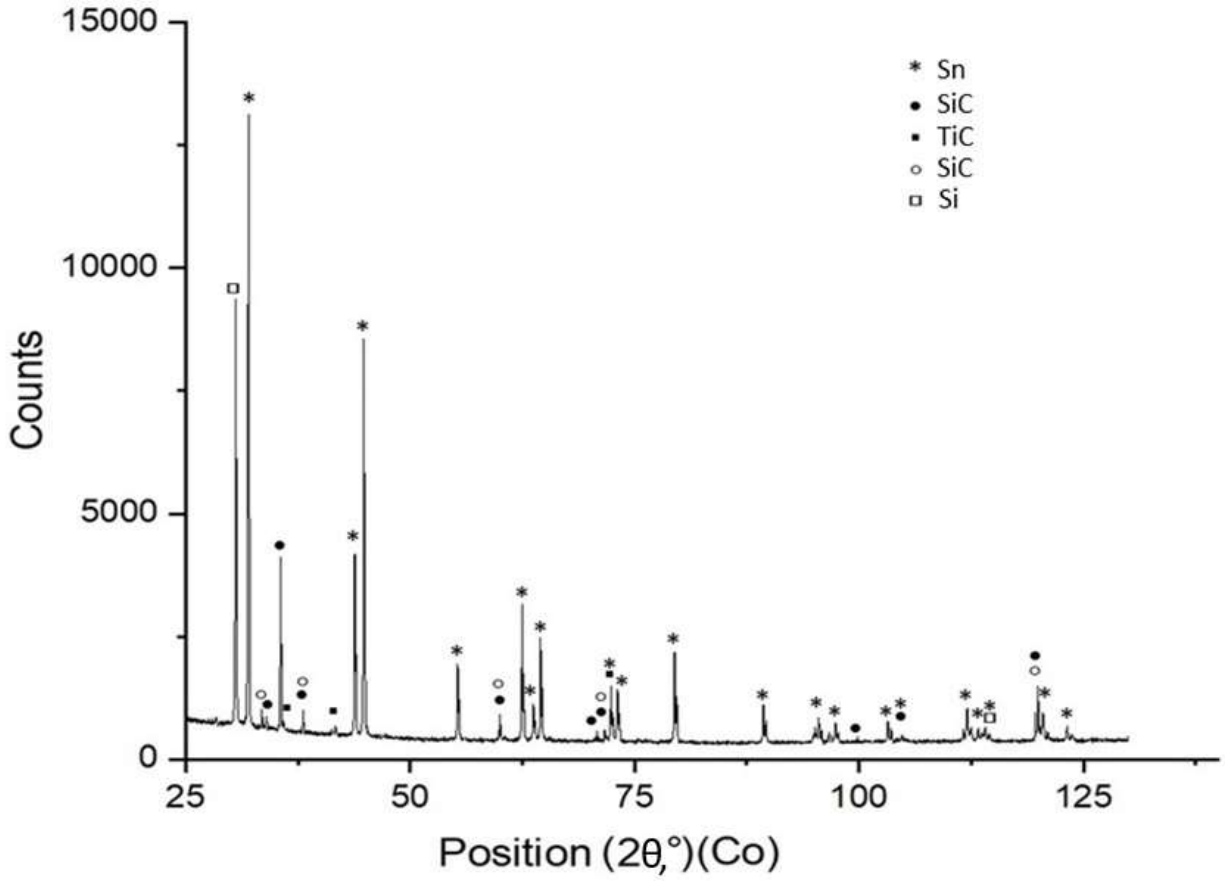

Figure 6. XRD analysis of the solder SnTi3 with 6 wt.% SiC nanoparticles.

3.3. Tensile strength of the solder alloy

Mechanical tests aimed to measure the tensile strength of the active soldering alloy SnTi3 with 6 wt.% SiC nanoparticles. The dimensions of the test pieces were designed and calculated. The loading rate of each specimen was 1 mm/min. From the measured values, the average tensile strength in MPa was calculated; results are given in Figure 7.

The solder SnTi3 with 3 wt.% SiC nanoparticles attained a tensile strength of 17.8 ± 0.2 MPa and ductility of 74.6% ± 8.5%; therefore, the solder SnTi3 + 6 wt.% SiC nanoparticles provided better mechanical properties. An increased SiC nanoparticle content led to a 2.8% increase in tensile strength while doubling the ductility (by 104%). This increased ductility may be an advantage in applications where resistance against brittle failure is required.

Such an improvement in mechanical properties makes the solder type SnTi3 + 6 wt.% SiC nanoparticles more suitable for practical industrial applications where tensile strength, but mainly higher material ductility, is desirable.

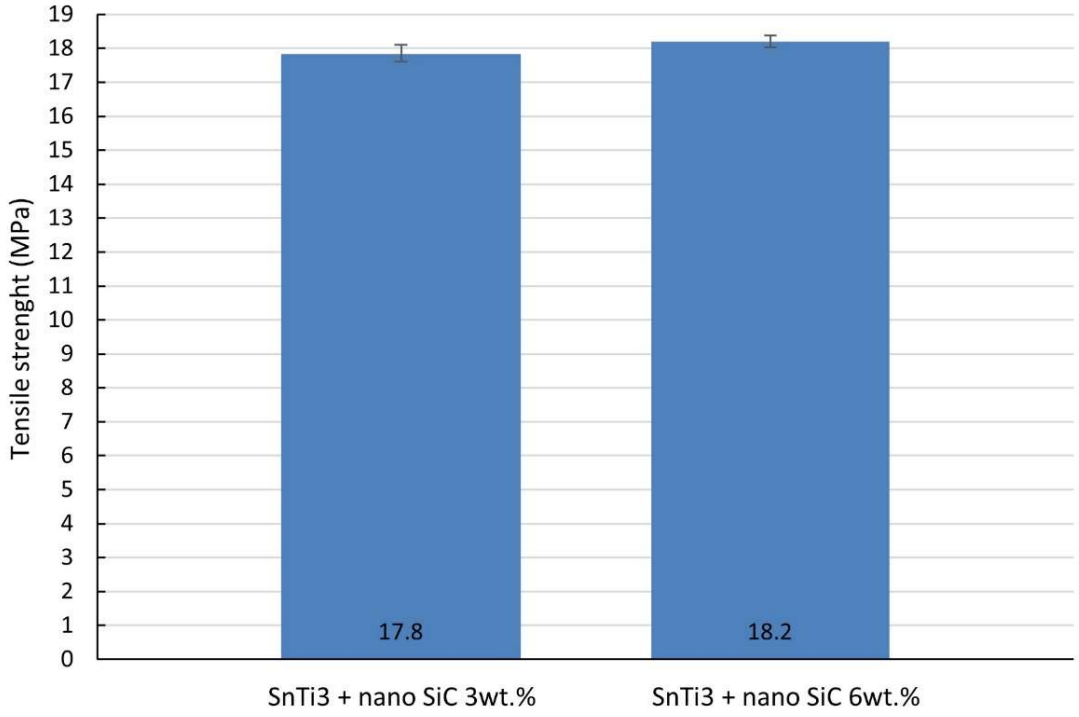

Figure 7. Tensile strength of experimental soldering alloys.

3.4. Analysis of the transition zone of the soldered joint between SiC substrate/solder type SnTi3 + 6 wt.% SiC nanoparticles

For the determination of the chemical composition and identification of individual phases, the SEM/EDX analysis was performed. The transition zone between the SiC substrate and the solder SnTi3 + 6 wt.% SiC nanoparticles was analyzed in detail (Figure 8). Spectra 1–5 were analyzed and are described in Table 4. Spectrum 1 represents the particles of unmolten titanium in the solder matrix. In Spectrum 2, a high Ti content was measured, related to the Ti_3Sn phase. Spectrum 3 represents the solder zone (matrix). Due to convection and diffusion in the melt, an increased concentration of Cu in (Sn) occurred. The mixture of solid solution (Sn) + η Cu_6Sn_5 phase (minority proportion) was also observed. In the case of Spectrum 4, SiC nanoparticles were observed in the solder. This analysis also captured the surrounding zone, and the presence of Cu (1 at.%) in the solder was observed. The analysis of Spectrum 5 showed zones of ceramic substrate (SiC).

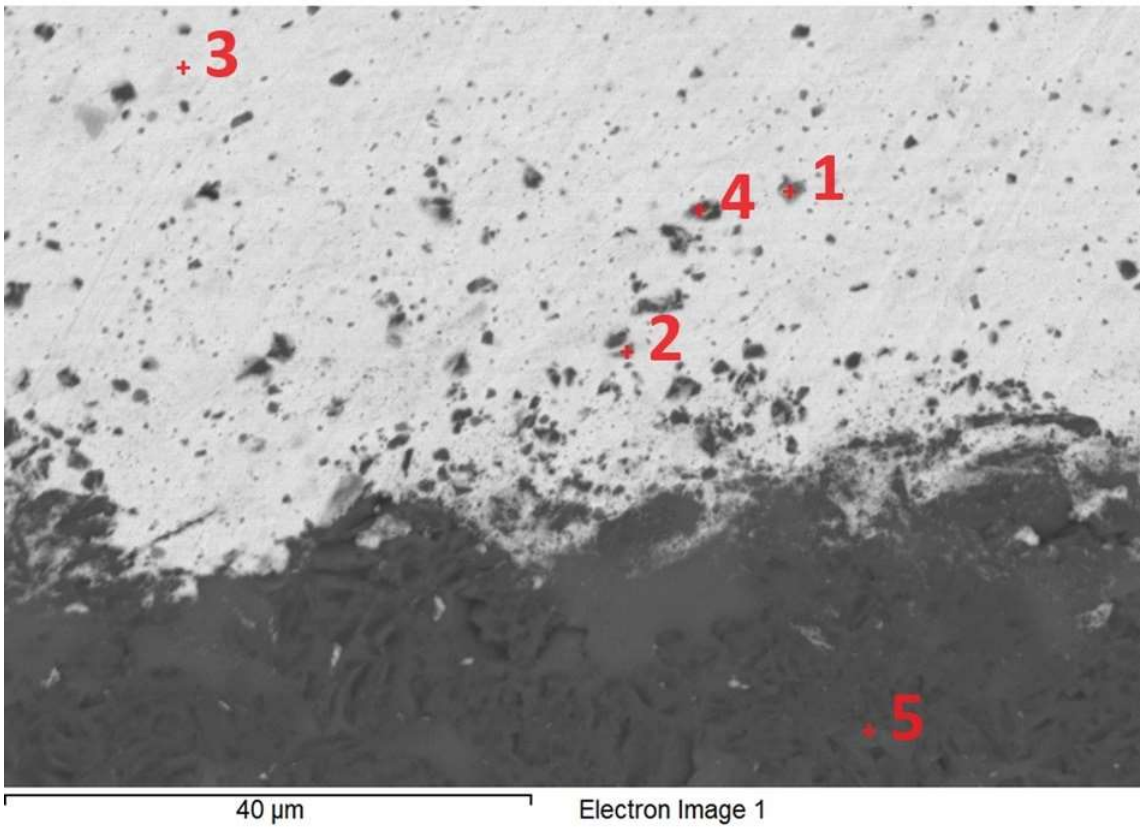

Figure 8. EDX point analysis of the joint of SiC/SnTi3 + 6 wt.% SiC nanoparticles.

Table 4. Results from the point energy-dispersion analysis of SiC/SnTi3 + 6 wt.% SiC nanoparticles.

Spectrum	Si (at.%)	Ti (at.%)	Cu (at.%)	Sn (at.%)	Solder component
1	0.24	93.02	0.66	6.08	Participle Ti
2	3.66	77.91	4.24	14.19	Phase Ti_3Sn
3	1.53	-	10.28	88.19	Solid solution mixture (Sn) + phase Cu_6Sn_5
4	86.08	-	1.06	12.86	Nanoparticles SiC
5	99.59	0	0	0.41	Substrate SiC

From Figure 9, it is clear that titanium phases are formed in the solder matrix. The distribution of Sn, Si, and Cu elements after soldering is documented by the map in Figure 9. An undulated boundary was formed on the boundary between the SiC substrate and the solder, corresponding to the effect of ultrasonic power.

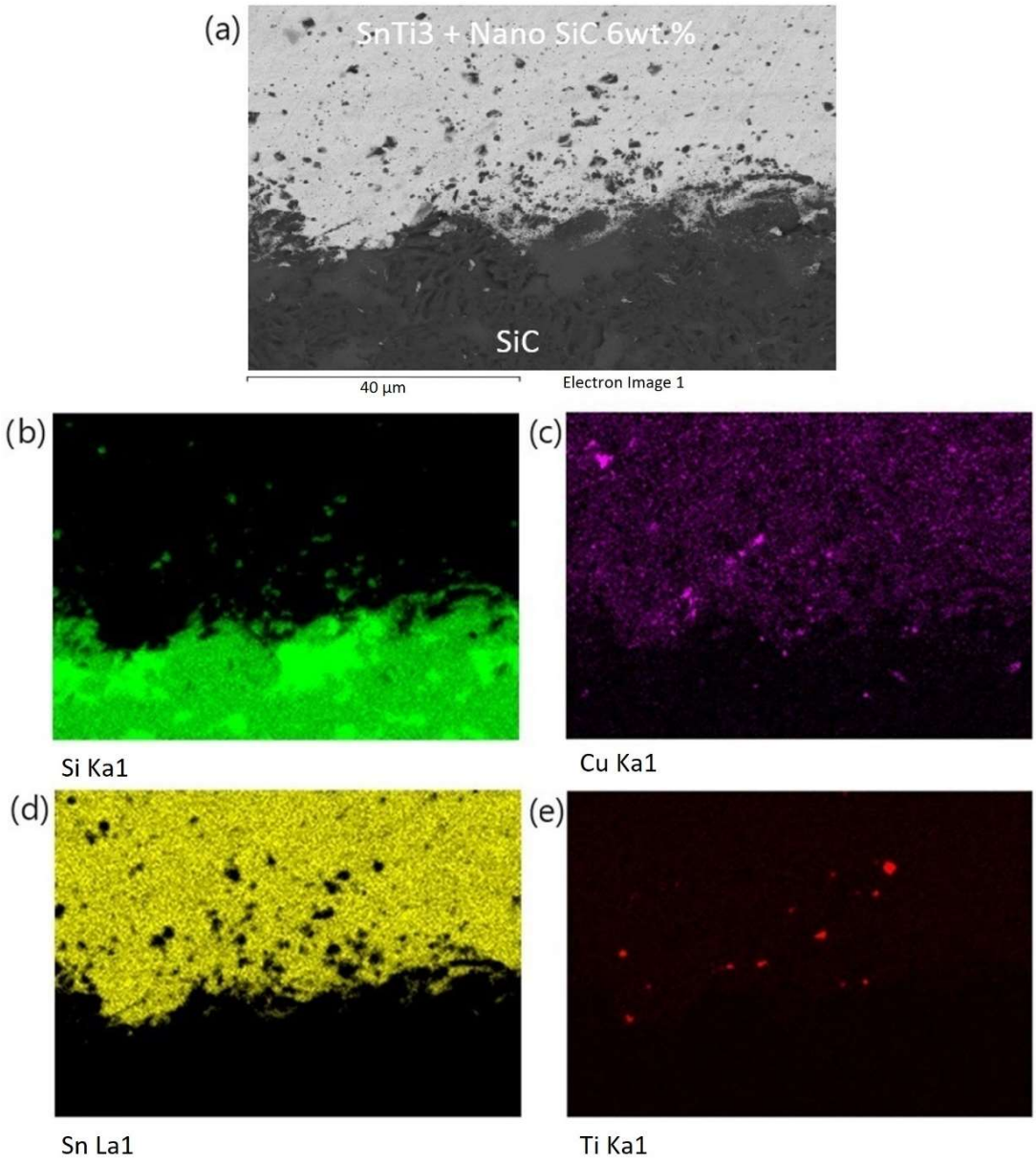

Figure 9. Planar distribution of elements on the boundary of SiC/SnTi3 + 6 wt.% SiC nanoparticles: (a) joint microstructure; (b) Si; (c) Cu; (d) Sn; (e) Ti.

3.5. Analysis of the transition zone of the soldered joint between SnTi3 with 6 wt.% SiC nanoparticles and Cu substrate

On the transition zone between the SnTi3 + 6 wt.% SiC nanoparticles and the Cu substrate, an undulated boundary was observed, corresponding to the effect of ultrasonic power (Figure 10). Spectra 1–5, given in Table 5, were analyzed; Spectrum 1 showed heterogeneous zones, together with the presence of SiC nanoparticles. The proportion of Ti:Cu:Sn elements was variable, with the following plausible phases: ternary (CuSnTi [22] or $CuSnTi3_5$ [23]) and binary in Figure 11 (η Cu_6Sn_5, Cu_3Sn, Sn_5Ti_6, $SnTi3_2$, $SnTi_3$, Cu_4Ti_3, Cu_4Ti, Cu_2Ti, and CuTi). The measurement of Spectrum 2 revealed a zone of copper substrate. The presence of SiC nanoparticles was observed in a minor amount.

The grey zones in Spectrum 3 represent the intermetallic phase of η Cu_6Sn_5, in agreement with the binary diagram Cu–Sn. Spectrum 4 represents the mixture of the solid solution (Sn) with η Cu_6Sn_5 phase. Spectrum 5 represents the SiC nanoparticles in the solder. This analysis also captured the surrounding zone of the solder.

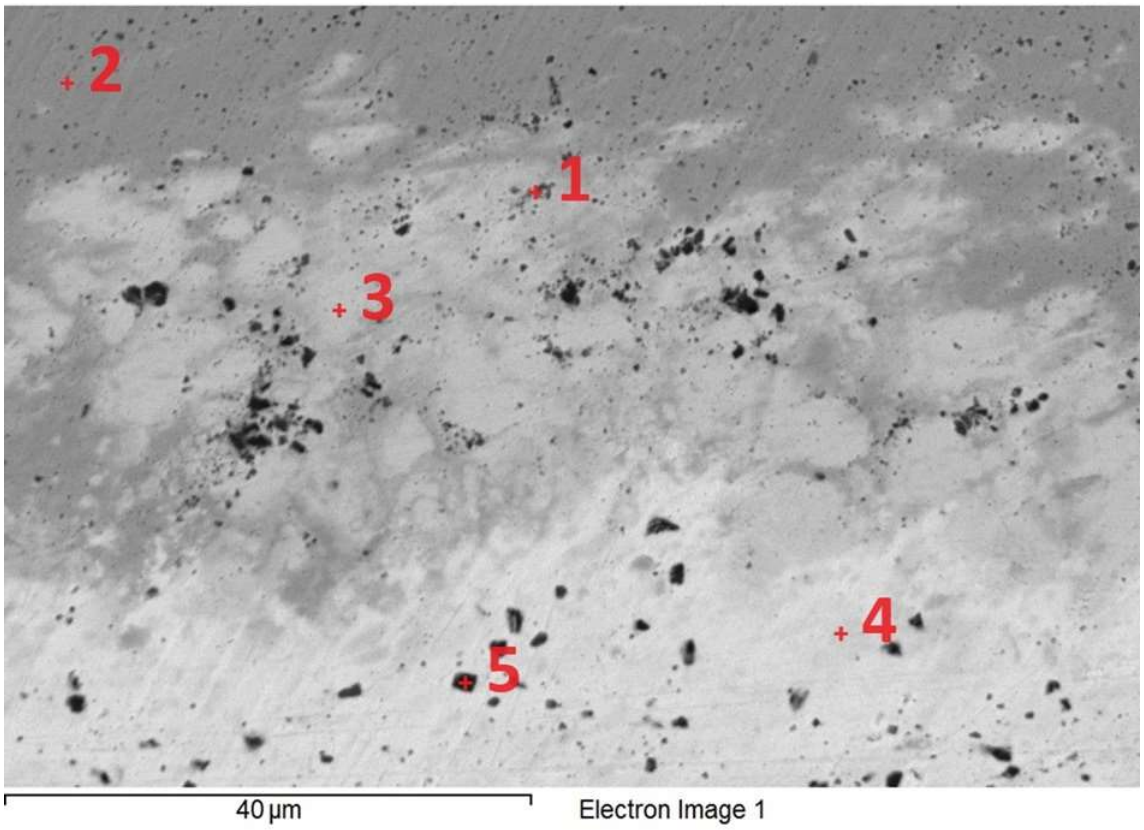

Figure 10. EDX point analysis of the SnTi3 + 6 wt.% SiC nanoparticles/Cu substrate.

Table 5. Results from the point energy-dispersion analysis of SnTi3 + 6 wt.% SiC nanoparticles/Cu substrate.

Spectrum	Si (at.%)	Ti (at.%)	Cu (at.%)	Sn (at.%)	Solder component
1	9.16	19.41	50.53	20.9	-
2	0.9	0	98.54	0.56	Nanoparticle SiC
3	1	0	61.05	37.96	Intermetallic phase η Cu_6Sn_5
4	1	0	37.12	61.88	Solid solution mixture (Sn) + phase η Cu_6Sn_5
5	82.94	0	0.43	16.63	Nanoparticle SiC

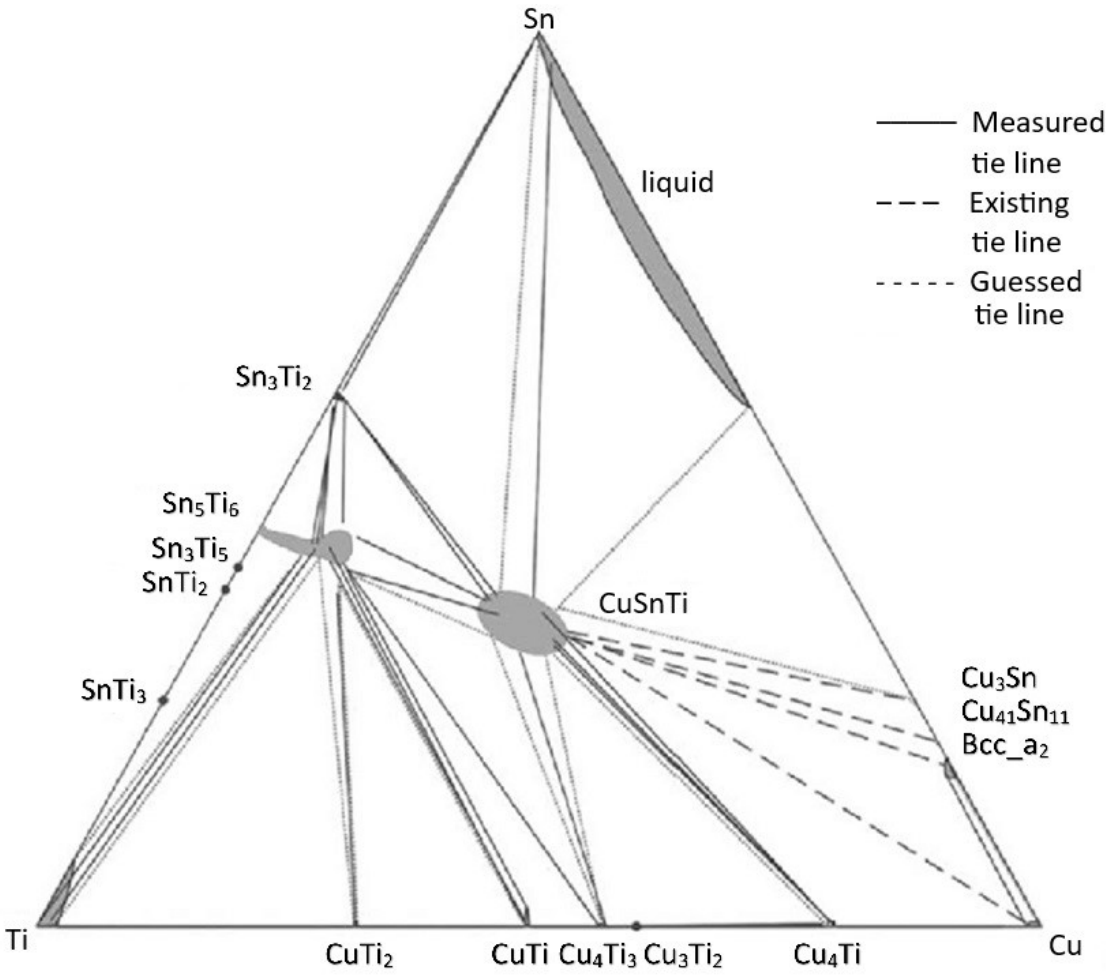

Figure 11. Phase equilibria of the Cu-Sn-Ti ternary system at 823 K.

The distribution of individual elements across the boundary between the SnTi3 solder with 6 wt.% SiC nanoparticles and the Cu substrate is clearly visible and mainly consists of a uniformly formed solder matrix. The formation of elements on the joint boundary can be observed in colors in Figure 12.

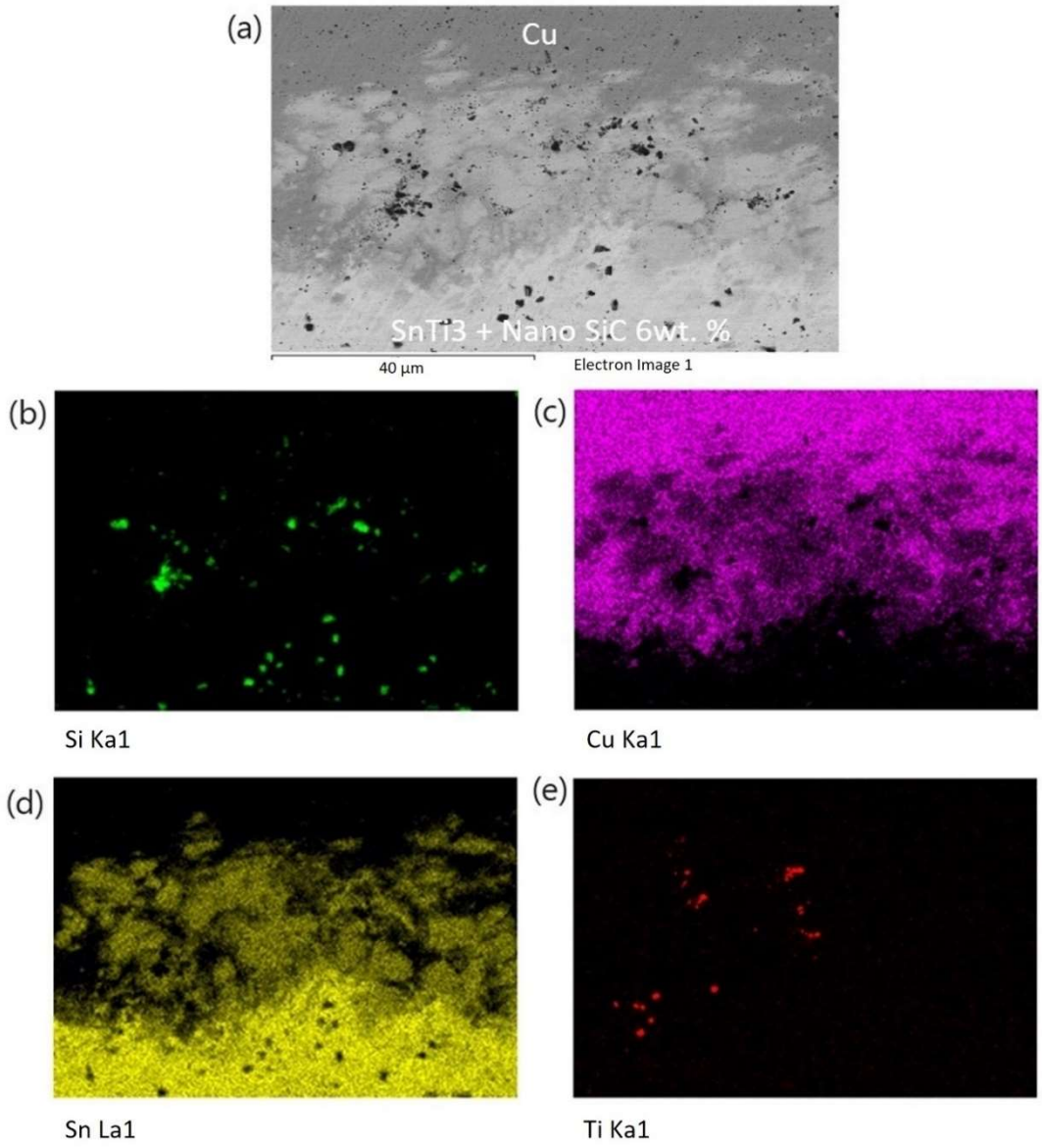

Figure 12. Planar distribution of elements on the boundary between the SnTi3 solder with 6 wt.% of SiC nanoparticles and the Cu substrate: (a) joint microstructure; (b) Si; (c) Cu; (d) Sn; (e) Ti.

The line analysis in Figure 13 represents the concentration profiles across the boundary of the SnTi3 solder with 6 wt.% SiC nanoparticles with the Cu substrate in an overall length of 40 µm. Figure 13a shows an electron image of zones with marked line analyses. The upper part shows the Cu substrate; the lower part shows the SnTi3 solder with 6 wt.% SiC nanoparticles. The mixing of solder and substrate is clearly seen, indicating the formation of interphase zones. Figure 13b–e shows the distribution of Si, Sn, Ti, and Cu elements across the analyzed zone.

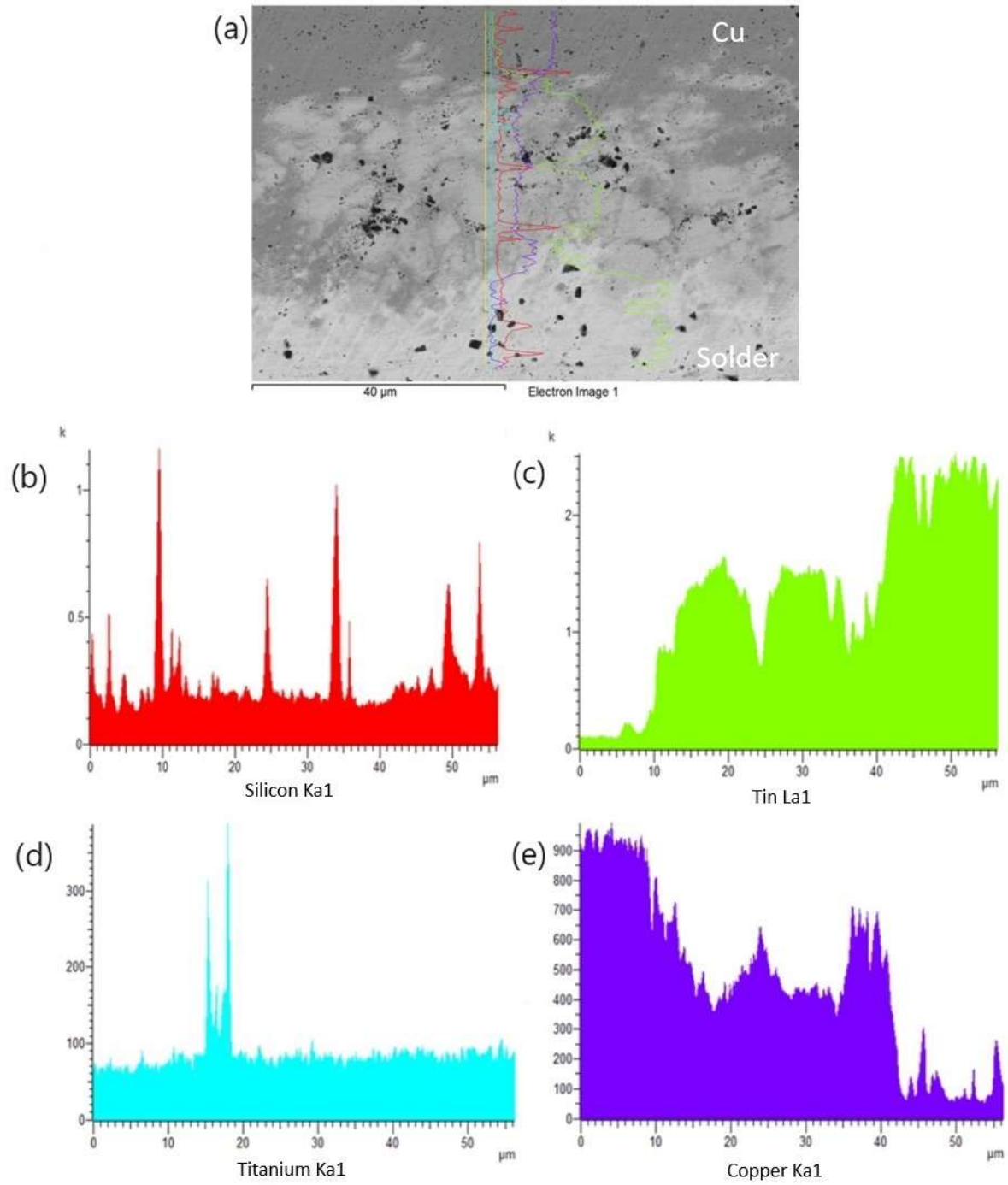

Figure 13. Line EDX analysis of the SnTi3 solder with 6 wt.% SiC nanoparticles and Cu joint: (a) joint microstructure; (b) Si; (c) Sn; (d) Ti; (e) Cu.

3.6. Shear strength of soldered joints

Here, research was focused on soldering SiC ceramics and Cu substrate. The aim of this study was to assess the suitability of an active solder of SnTi3 + 6 wt.% SiC nanoparticles. The measurement was performed on three specimens.

In the studied combination of SiC ceramics and Cu substrate with an application of SnTi3 solder with 6 wt.% SiC nanoparticles, an average shear strength of 21.5 MPa (Figure 14) was achieved. Due to the versatility of this solder and its potential practical applications, shear testing was also extended to other ceramic materials: Al_2O_3, AlN, Si_3N_4, SiC, and ZrO_2.

The best results were achieved with SiC/Cu and ZrO_2/Cu specimens, with a shear strength of 21.5 MPa. This suggests that these ceramic materials are the most suitable for soldering with Cu substrate by using an active SnTi3 solder with 6 wt.% SiC nanoparticles.

Based on the results, the SnTi3 + 6 wt.% SiC solder can be recommended for applications where higher shear strength is necessary, mainly for soldering SiC and ZrO_2 ceramics with Cu substrate. These materials show the best mechanical properties and are most suitable for practical industrial applications.

The combination of soldering materials such as SiC/Cu is an excellent choice when high shear strength is desirable. The SiC/Cu proved to be a better combination for those applications than ZrO_2/Cu. The soldered joints of SiC/Cu and ZrO_2/Cu offer comparable strength values.

The mechanical properties and joining mechanisms of the investigated SnTi3 solder with 6 wt.% SiC nanoparticles can be compared with that of other conventional solders such as Sn58Bi or Sn-Ag composites, which are often used in similar applications. For example, the addition of SiC nanoparticles to a Sn58Bi solder increased shear strength by 6% [16]. This result is comparable to the improvement achieved in this work (21.5 MPa), where the added SiC nanoparticles contributed significantly to the improvement of the mechanical properties of the joints. In addition, similar mechanical improvements are also observed for Sn-Ag composites, where the addition of nanoparticles improves the strength of the joints and reduces the growth of intermetallic compounds. Comparison of the formation mechanisms of phases such as TiC and Cu_6Sn_5 shows that these phase transformations significantly affect the resulting mechanical behavior of the joints and their long-term reliability.

These characteristics make the SiC/Cu combination an optimum choice for demanding conditions, where long-term reliability and efficiency are desired, as well as for a wide range of industrial applications, including electronics, automotive industry, aviation, and power engineering.

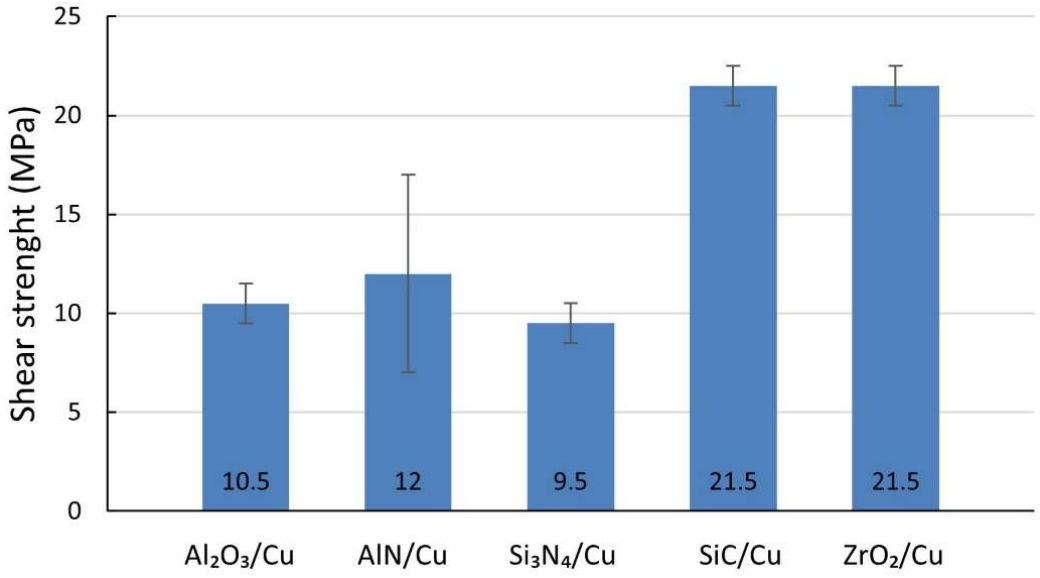

Figure 14. Shear strength of soldered joints fabricated by use of SnTi3 + nanoparticles SiC 6 wt.% solder.

3.7. Analysis of the fractured surface

The analysis of the fractured surface was performed from the side of SiC and is documented in Figure 15, which shows the surface of the boundary between the SnTi3 solder with 6 wt.% SiC nanoparticles and the Cu substrate. The fractured surface remained covered with the solder, suggesting that the fracture occurred in the solder probably due to a ductile fracture. The planar distribution of elements shows that Si and C are concentrated in SiC zones, while Sn, Ti, and Cu are concentrated in the zone of solder and substrate. Such a distribution of elements proves an interaction between the solder and the substrate, which may affect the joint properties.

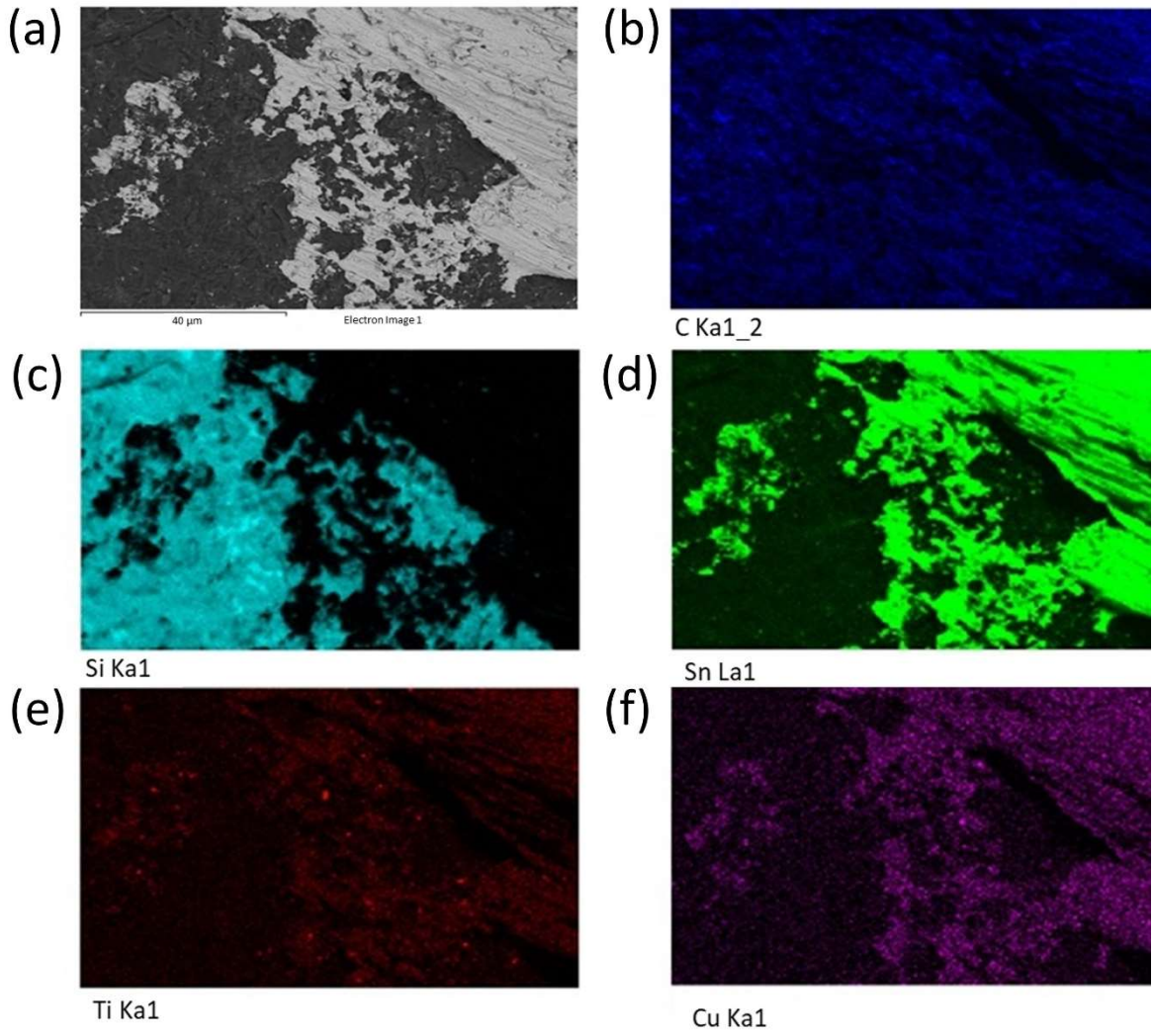

Figure 15. Fractured surface of the solder SnTi3 with 6 wt.% SiC nanoparticles and Cu substrate and the planar distribution of individual elements: (a) fracture morphology; (b) C; (c) Si; (d) Sn; (e) Ti; (f) Cu.

Analysis of the fracture surfaces indicates that ductile fracture was the dominant failure mechanism; however, the presence of SiC nanoparticles and phases such as TiC may influence the failure mechanisms under different loading conditions. These phases typically act as barriers to crack

propagation, thereby improving the toughness of the solder. Nevertheless, at higher concentrations, they can lead to localized brittle fracture. The presence of these phases can alter the behavior of the joint, especially under repeated loading or thermal cycling, which can lead to combined fracture mechanisms where ductile fracture occurs in the solder and brittle fracture occurs in areas rich in intermetallic phases and SiC nanoparticles.

For a more precise identification of the mechanism of bond formation, an XRD analysis of the fractured surface of the SnTi3 + 6 wt.% SiC nanoparticles/Cu joint was performed (Figure 16). On the fractured surface, Ti_2Sn, CuSn, TiC, CTi_2, and Cu_6Sn_5 phases were identified; the TiC and CTi_2 phases are the result of the interaction between an active Ti from the solder and the surface of the ceramic material (SiC). The CuSn and Cu_6Sn_5 phases are the result of the interaction between the tin from the solder and the copper substrate.

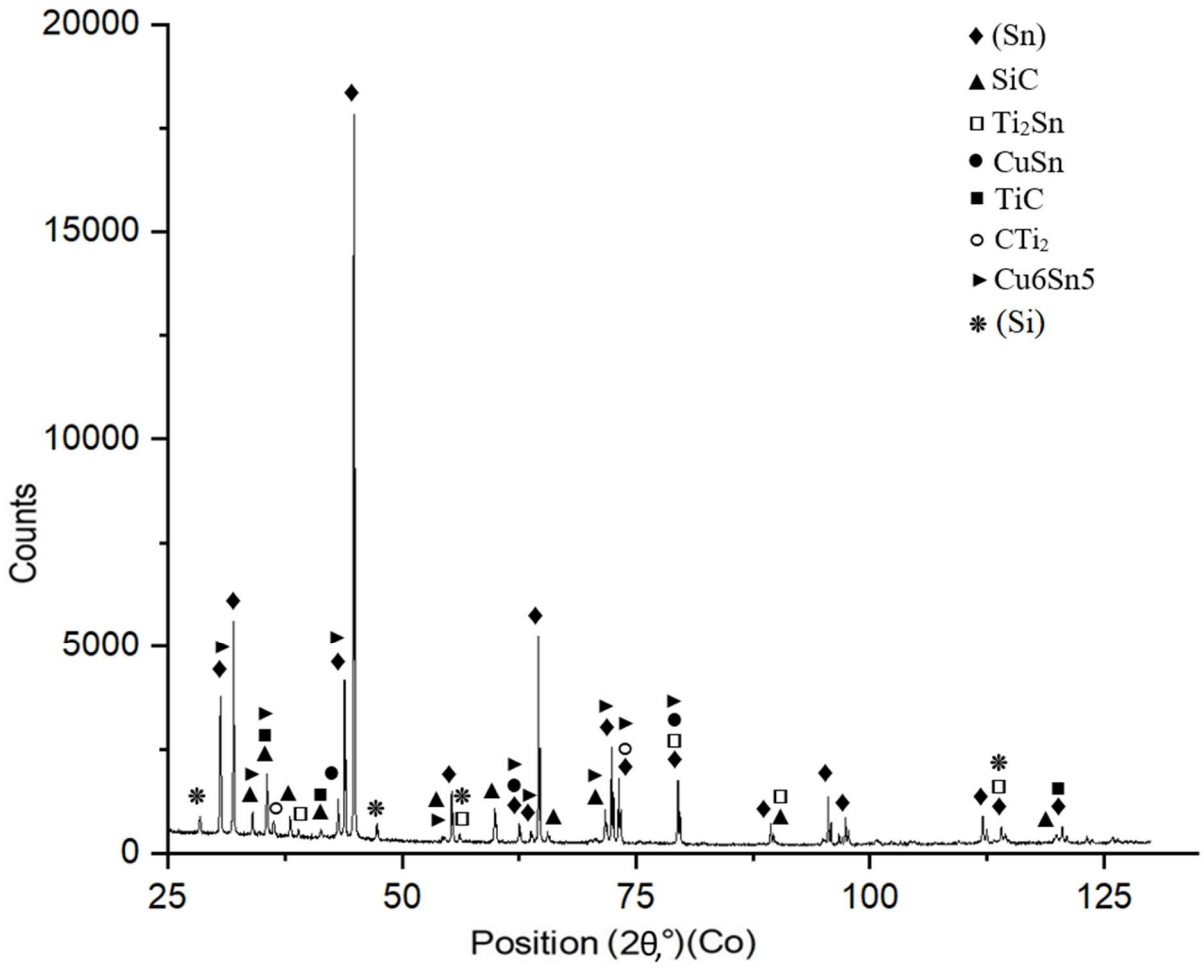

Figure 16. XRD analysis of the fractured surface of the SnTi3 solder with 6 wt.% SiC nanoparticles/Cu joint.

4. Conclusions

The aim of this study was to analyze the active solder SnTi3 with 6 wt.% SiC nanoparticles, destined for soldering the combination of SiC ceramics and Cu substrate. To enhance the wettability

of the ceramic material with solder, a soldering process with an active ultrasound was applied. The results can be characterized as follows:

- For the determination of the melting point of the solder alloy, TG/DTA analysis was applied. This analysis proved the occurrence of two transformations at temperatures of 234 and 244 °C; the former corresponded to the eutectic reaction in the Sn-Ti system, and the latter was the liquidus temperature.
- The microstructure of SnTi3 + 6 wt.% SiC nanoparticles consisted of a tin matrix, where the SiC nanoparticles and TiC phase are distributed, which was proved by EDX analysis.
- The tensile strength of the SnTi3 + 6 wt.% SiC nanoparticles varied from 18.0 to 18.4 MPa.
- The bond between SiC ceramics and the solder was formed due to their interaction via diffusion and chemical reaction, which led to the formation of TiC and CTi_2 phases.
- An undulated boundary formed on the interface between the solder and the Cu substrate, corresponding to the effect of ultrasonic power. The bond was formed by the intermetallic η-Cu_6Sn_5 phase and the solid solution (Sn). Also, the formation of ternary phases CuSnTi or $CuSnTi3_5$ may be assumed.
- The average shear strength of the SiC/Cu joint fabricated using SnTi3 + 6 wt.% SiC nanoparticles was 21.5 MPa. A similar shear strength was achieved with the ZrO_2/Cu joint. In other assessed ceramic materials, an average shear strength of 10 MPa was obtained.

Use of AI tools declaration

The authors declare they have not used Artificial Intelligence (AI) tools in the creation of this article.

Acknowledgments

This work was supported by the Slovak Research and Development Agency under the contract no. APVV-21-0054 and no. APVV-17-0025. The paper was also prepared with the support of VEGA 1/0237/24: Research of active soldering alloys filled with ceramic material nanoparticles, and VEGA 1/0026/23: Modification of the structure and mechanical properties of soldering alloys to increase the reliability of soldered joints in advanced electronic applications.

Author contributions

Conceptualisation: R.K. and T.M.; methodology: R.K.; validation: R.K., T.M. and J.D.; formal analysis: J.D., P.G. and M.P.; investigation: R.K. and T.M.; data analysis: T.M. and M.S; typing—initial draft preparation: R.K.; typing—review and editing: T.M.; visualization: T.M.; supervision: R.K.; project administration: T.M. All authors have read and agreed to the published version of the manuscript.

Conflict of interest

All authors declare no conflicts of interest in this paper.

References

1. Sonawane PD, Raja VKB, Palanikumar K, et al. (2021) Effects of gallium, phosphorus and nickel addition in lead-free solders: A review. *Mater Today Proc* 46: 3578–3581. https://doi.org/10.1016/j.matpr.2021.01.335
2. Li CJ, Yan YF, Gao TT, et al. (2021) The influence of Ag on the microstructure, thermal properties and mechanical behavior of Sn-25Sb-xAg high temperature lead-free solder. *Vacuum* 185: 110015. https://doi.org/10.1016/j.vacuum.2020.110015
3. Vafaeenezhad H, Seyedein SH, Aboutalebi MR, et al. (2019) Creep life prediction for Sn-5Sb lead-free solder alloy: Model and experiment. *Microelectron Eng* 207: 55–65. https://doi.org/10.1016/j.mee.2019.01.006
4. Chang S, Lin S, Hsieh K (2007) Phase reaction in Sn-9Zn solder with Ni/Au surface finish bond-pad at 175 °C ageing. *J Alloys Compd* 428: 179–184. https://doi.org/10.1016/j.jallcom.2006.01.106
5. Kim D, Jung S (2005) Interfacial reactions and growth kinetics for intermetallic compound layer between In-48Sn solder and bare Cu substrate. *J Alloys Compd* 386: 151–156. https://doi.org/10.1016/j.jallcom.2004.05.055
6. Jayesh S, Elias J (2020) Investigations on the properties of new lead free alloy composition—Sn-0.5Cu-3.5Bi. *Mater Today Proc* 21: 329–331. https://doi.org/10.1016/j.matpr.2019.05.455
7. Yang L, Ma S, Mu G (2021) Improvements of microstructure and hardness of lead-free solders doped with Mo nanoparticles. *Mater Lett* 304: 130654. https://doi.org/10.1016/j.matlet.2021.130654
8. Shen Y, Chen S, Chen H, et al. (2021) Extremely thin interlayer of multielement intermetallic compound between Sn-based solders and FeCoNiMn high-entropy alloy. *Appl Surf Sci Adv* 558: 149945. https://doi.org/10.1016/j.apsusc.2021.149945
9. Kanlayasiri K, Ariga T (2015) Physical properties of Sn58Bi-xNi lead-free solder and its interfacial reaction with copper substrate. *Mater Design* 86: 371–378. https://doi.org/10.1016/j.matdes.2015.07.108
10. Khodabakhshi F, Zareghomsheh M, Khatibi G (2020) Nanoidentation creep properties of lead-free nanocomposite solders reinforced by modified carbon nanotubes. *Mater Sci Eng A* 797: 140203. https://doi.org/10.1016/j.msea.2020.140203
11. Jung D, Sharma A, Jung J (2018) Influence of dual ceramic nanomaterials on the solderability and interfacial reactions between lead-free Sn-AgCu and a Cu conductor. *J Alloys Compd* 743: 300–313. https://doi.org/10.1016/j.jallcom.2018.02.017
12. Zhang L, Tu K (2014) Structure and properties of lead-free solders bearing micro and nano particles. *Mater Sci Eng R* 82: 1–32.
13. Pal M, Gergely G, Koncz-Horváth D, et al. (2021) Investigation of microstructure and wetting behavior of Sn-3.0Ag-0.5Cu (SAC305) lead-free solder with additions of 1.0 wt% SiC on copper substrate. *Intermetallics* 128: 106991. http://dx.doi.org/10.1016/j.intermet.2020.106991
14. Koleňák R, Kostolný I, Drapala J, et al. (2021) Characterization of Sn–Sb–Ti solder alloy and the study of its use for the ultrasonic soldering process of SiC ceramics with a Cu–SiC metal–ceramic composite. *Materials* 14: 1–22. https://doi.org/10.3390/ma14216369
15. Chen S, Zhang L, Liu J, et al. (2010) A reliability study of nanoparticles reinforced composite lead-free solder. *Mater Trans* 51: 1720–1726. https://doi.org/10.2320/matertrans.MJ201002

16. Hu X, Xu H, Chen W, et al. (2021) Effects of ultrasonic treatment on mechanical properties and microstructure evolution of the Cu/SAC305 solder joints. *J Manuf Process* 64: 648–654. https://doi.org/10.1016/j.jmapro.2021.01.045
17. Shin YS, Lee S, Yoo S, et al. (2009) Mechanical and microstructural properties of SiC-mixed Sn-Bi composite solder bumps by electroplating. European Microelectronics and Packaging Conference, Rimini, Italy, 1–4.
18. Jiang N, Zhang L, Liu ZQ, et al. (2019) Influences of doping Ti nanoparticles on microstructure and properties of Sn58Bi solder. *J Mater Sci Mater Electron* 30: 17583–17590. https://doi.org/10.1007/s10854-019-02107-0
19. Wang HZ, Hu XW, Jiang XX (2020) Effects of Ni modified MWCNTs on the microstructural evolution and shear strength of Sn-3.0Ag-0.5Cu composite solder joints. *Mater Charact* 163: 110287. https://doi.org/10.1016/j.matchar.2020.110287
20. Lee A, Subramanian KN, Lee JG (2005) Development of nanocomposite lead-free electronic solders. Proceedings of the International Symposium on Advanced Packaging Materials: Processes, Properties and Interfaces, Irvine, CA, USA, 2005, 276–281. https://doi.org/10.1109/ISAPM.2005.1432089
21. He QQ, Zhang YB, Duan N, et al. (2020) Wetting behaviours and interfacial characteristics of Co-binder sintered polycrystalline diamond by SnTi active solder. *Powder Technol* 376: 643–651. https://doi.org/10.1016/j.powtec.2020.08.079
22. Zhou GJ, Zhou Y, Luo Y (2017) Phase equilibria of the Cu-Sn-Ti ternary system at 823K. *AIP Adv* 7: 025118. https://doi.org/10.1063/1.4975220
23. Hsieh Y, Lin S (2008) Microstructural development of Cu–Sn–Ti alloys on graphite. *J Alloys Compd* 466: 126–132. https://doi.org/10.1016/j.jallcom.2007.11.038

AIMS Press